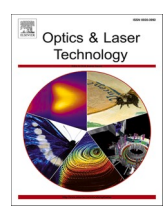
ELSEVIER

Contents lists available at ScienceDirect

Optics and Laser Technology

journal homepage: www.elsevier.com/locate/optlastec



Full length article



Tunable chromatic dispersion based on uniform fiber Bragg gratings in helical multicore fiber inscribed by femtosecond laser

Yanjie Meng ^{a,b,c}, Wenfa Liang ^{a,c}, Zhenwei Peng ^{a,c}, Shuai Xiao ^{a,c}, Rongyi Shan ^{a,c}, Huajian Zhong ^{a,c}, Yuhao Kong ^{a,c}, Cailing Fu ^{a,c}, Changrui Liao ^{a,c}, Zhicai Zhang ^d, Yiping Wang ^{b,*}

- a Key Laboratory of Optoelectronic Devices and Systems of Ministry of Education/GuangDong Province, College of Physics and Optoelectronic Engineering, Shenzhen University, Shenzhen 518060, China
- ^b Guangdong Laboratory of Artificial Intelligence and Digital Economy (SZ), Shenzhen 518107, China
- ^c Shenzhen Key Laboratory of Photonic Devices and Sensing Systems for Internet of Things, Guangdong and Hong Kong Joint Research Centre for Optical Fibre Sensors, Shenzhen University, Shenzhen 518060, China
- ^d China Nonferrous Metal (Guilin) Geology and Mining Co., Ltd., Guilin 541004, China

ARTICLE INFO

Keywords: Chirped fiber Bragg grating Multicore fiber Femtosecond laser manufacture Fiber optics communications

ABSTRACT

A novel method for controlling the chromatic dispersion of uniform fiber Bragg gratings (FBGs) in helical multicore fiber (HMCF) is proposed and experimentally demonstrated. By precisely manipulating the 3D shape of the grating, including local curvature and bending orientation, varying strain gradients are induced, leading to tunable bandwidth and group delay. FBGs were inscribed in HMCF using the femtosecond laser point-by-point (PbP) technique. When the grating was shaped into an arc with a radius of 1 cm, a tuning bandwidth of 8.3 nm and a dispersion of 5.7 ps/nm were achieved. Furthermore, a misalignment fabrication method is introduced, ensuring that gratings in different cores exhibit consistent tunable dispersion characteristics through curvature adjustment. This proposed method offers significant potential for chromatic dispersion control in optical transmission systems based on multicore fiber.

1. Introduction

The use of multicore fiber (MCF) for space division multiplexing (SDM) is a significant approach to increasing transmission capacity in optical networks [1,2]. Following Moore's Law, future expansions in transmission capacity are expected. In addition to SDM, single-mode fiber (SMF) transmission capacity has been enhanced by leveraging various multiplexing techniques, such as polarization and wavelength division multiplexing (WDM) [3,4]. Notably, in 2024, a record-breaking data rate of 402.2 Tb/s was achieved using WDM in SMF [5]. A combination of SDM and WDM has been employed to further sustain the growth in optical transmission system capacity [6,7].

In WDM systems, dispersion plays a critical role. On one hand, fiber dispersion leads to pulse broadening and inter-symbol interference, reducing the communication capacity. On the other hand, over long transmission distances, dispersion exacerbates pulse broadening, thereby limiting transmission range. Therefore, dispersion

compensation is essential. Chirped fiber Bragg gratings (CFBGs) have been widely adopted as dispersion compensators due to their fiber compatibility, compact size, low nonlinearity, and minimal insertion loss [8,9]. Various techniques have been proposed for tuning CFBG dispersion, including thermal tuning via heaters [10,11], tapered fiber methods [12,13], and symmetric bending of flexible cantilever beams [14–17]. However, all these tunable dispersion compensators have been designed for use with SMF.

FBGs can be inscribed in MCF using ultraviolet (UV) laser or femtosecond laser methods. The traditional approach relies on UV laser combined with a phase mask (PM) to inscribe uniform or chirped gratings in MCF [18–21]. Although this method is technically mature and offers advantages such as low insertion loss and minimal polarization-dependent loss, it is prone to shadowing effects due to UV absorption and lensing effect, which make it difficult to fabricate consistent gratings in multiple cores [18,19]. Additionally, the requirement for hydrogen loading and annealing before and after the process adds complexity and

E-mail address: ypwang@szu.edu.cn (Y. Wang).

^{*} Corresponding author.

time to the fabrication procedure [18,20,22].

In contrast, femtosecond laser direct-writing techniques, including point-by-point (PbP), line-by-line (LbL), and plane-by-plane (Pl-b-Pl) methods, offer a more flexible approach to grating inscription [23–26]. These methods enable high-precision control of 3D translation stages to inscribe gratings with varying Bragg wavelengths and complex spectral designs into different types of optical fibers. The fiber coating layer remains intact during the inscription process, and the fiber does not require hydrogen-loading, thereby preserving its mechanical strength. In 2018, A. Donko et al. successfully inscribed four uniform third-order FBGs in a seven-core fiber using the PbP method [27]. In 2019, Alexey Wolf et al. used the same method to inscribe uniform gratings in a helical seven-core fiber for vector bending sensing applications [28]. However, no studies have focused on the chromatic dispersion based on FBGs in MCF or the tunable dispersion mechanisms for such gratings.

In this paper, we proposed and experimentally demonstrated a method for controlling the chromatic dispersion of uniform FBGs in helical multicore fiber (HMCF). The FBGs were successfully fabricated in HMCF using the femtosecond laser PbP technique. The 3D shape of the fiber induces a strain gradient in the uniform gratings located on the outer core, allowing control over key grating properties such as bandwidth and group delay via adjustments to the local curvature and bending orientation. We systematically investigate the effects of bending orientation and curvature on the dispersion characteristics of the gratings in HMCF. Reflection spectra and group delay were measured by a coherent optical frequency domain reflectometry (OFDR). A tuning bandwidth of 8.3 nm and dispersion as low as 5.7 ps/ nm were achieved by shaping the grating into an arc with a 1 cm radius. Furthermore, we proposed and demonstrated a misalignment fabrication method to ensure that gratings in different cores exhibit consistent tunable dispersion characteristics, independent of bending orientation, and driven solely by curvature.

2. Fabrication and principle

2.1. Fabrication

As shown in Fig. 1, a femtosecond laser (Pharos PH1, Light Conversion) with a pulse width of 290 fs, central wavelength of 514 nm, and repetition rate of 200 kHz was used to inscribe uniform FBGs in a HMCF with a polymer coating layer via the PbP method [29]. This is beneficial for achieving higher-quality FBG. To precisely control the laser energy, a half-wave plate (HWP) in combination with a Glan prism was employed. The laser beam was focused by a $100\times$ oil-immersion objective lens (NA =1.33) and then directed into the fiber core. The HMCF was mounted

on a high-precision three-dimensional translation stage, secured with fiber holders. This stage allowed accurate movement of the fiber along the x-, y-, and z-axes, ensuring precise positioning relative to the laser focus. The OFDR has proven versatile in both time- and frequency-domain metrology, effectively analyzing FBG in the spectral and impulse response domains [30]. In this study, a commercial optical frequency domain reflectometer (OFDR) (LUNA, OBR4600) was used to measure the spectrum and group delay (GD) of each inscribed grating in the HMCF.

The grating fabrication process in HMCF followed these steps: In step 1, a section of HMCF with the polymer coating layer was secured using a pair of fiber holders on the 3D translation stage. A fan-in/out (FIFO) device was used to connect the SMF to one core of the HMCF, and the corresponding channel of the FIFO was linked to the OFDR. In step 2, the HMCF was carefully translated along the y- and z-axes to align the laser focus with the center of one of the fiber cores. In step 3, the three-dimensional coordinates of each point were calculated based on the geometric parameters of the HMCF and the period and length of the grating. The translation stage was then moved to the calculated coordinates, triggering the femtosecond laser to inscribe the grating.

In theory, if the precision of the translation stage is sufficiently high, the grating period can be set to very small values, allowing for the fabrication of chirped gratings with a wide range of chirp rates. However, in practice, the minimum achievable period is constrained by the translation stage's precision. To achieve finer tuning, small strains could be applied to the gratings, enabling further period modulation. By leveraging the relationship between the strain on the outer core and the 3D shape of the HMCF, a uniform FBG in the outer core can acquire versatile chirped characteristics.

2.2. Principle

Due to its circular cross-section and uniform density, MCF can be modeled as a linear Kirchhoff rod, with its mechanical behavior under bending governed by Euler-Bernoulli beam theory [31]. Specifically, the outer core of the HMCF is twisted around the central core with a certain pitch, causing the angle offset of the outer core to continuously change along the fiber axis. When the fiber is bent, as illustrated in Fig. 2(a), the strain in the outer core, denoted as ε_i , is expressed as:

$$\varepsilon_i = \kappa \bullet r_i cos \left(\theta_b - \theta_i^0 - \frac{2\pi}{h} s \right) \tag{1}$$

where r_i is the radial offset of the outer core from the fiber center, θ_i^0 is the angular offset from the local axis to the core at the initial position, h is the intrinsic twist pitch of the fiber, κ is the curvature of the fiber at

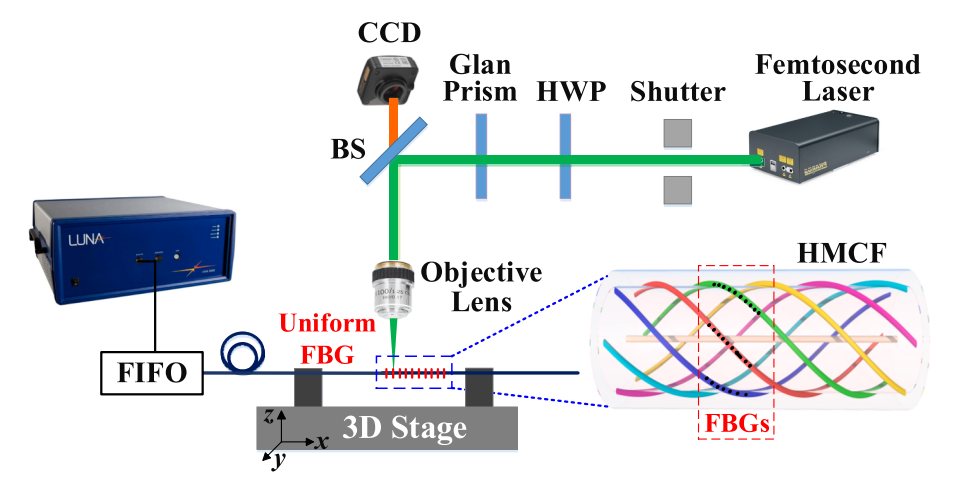


Fig. 1. Experimental setup for inscribing uniform FBGs in the HMCF using the femtosecond laser PbP technology, where an OFDR was used to measure spectrum and group delay of FBG.

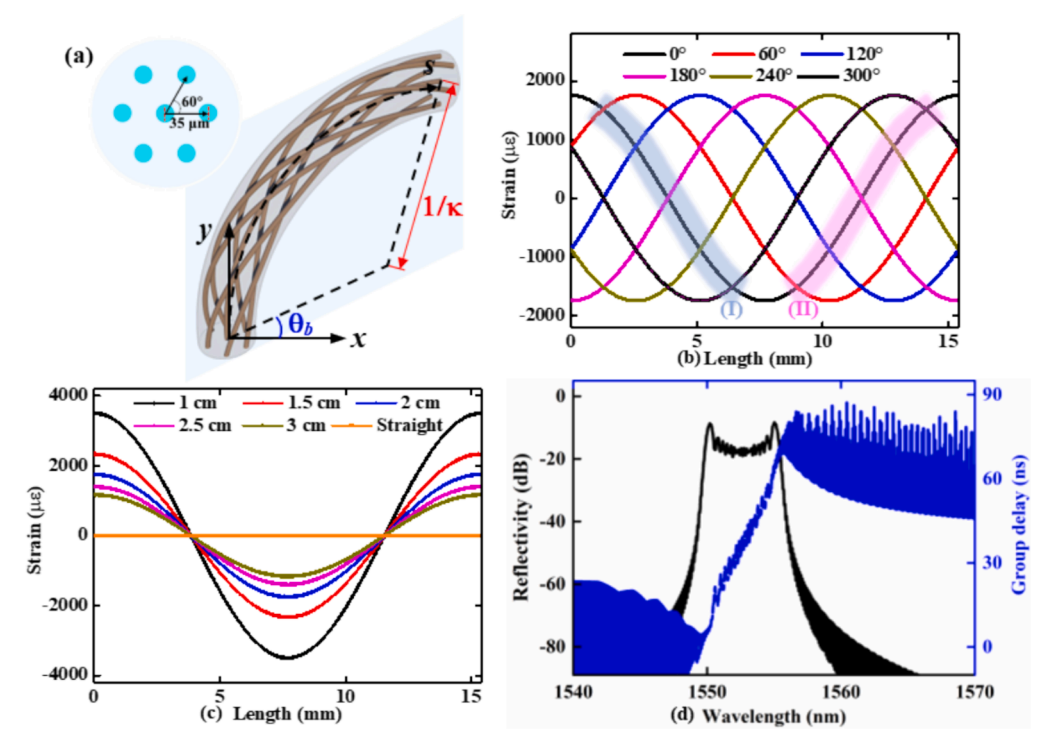


Fig. 2. (a) Schematic of a bending HMCF. Simulated strain distribution of HMCF under (b) different bending orientation and (c) curvature radius. (d) Simulated characteristics of a uniform grating under the strain gradient (I).

the arc length s, and θ_b is the bending orientation. As a result, the curvature and bending orientation define the fiber's 3D shape, inducing strain gradients along its length.

The strain distributions of the HMCF under different curvature and bending orientation were simulated. The HMCF used in this study consists of a central core and six outer cores arranged in a regular hexagon pattern. The geometrical parameters include a twist pitch of 15.4 mm and a core-to-core spacing of 35 µm. Strain distributions were simulated for a curvature radius of 2 cm, with bending orientation ranging from 0° to 360° , are shown in Fig. 2(b). While the maximum and minimum strain values remain constant, the stain profile shifts horizontally as the bending orientation changes. Additionally, strain distributions were simulated for a fixed bending orientation of 0° and curvature radii ranging from 1 cm to 3 cm, as shown in Fig. 2(c). In this case, the profile does not shift, but the maximum strain decreases as the curvature radius increases. When the fiber is straight, the strain is zero, resulting in no strain gradient. Thus, for a uniform grating under varying curvature and orientation, the grating period is no longer constant but varies along different positions of the fiber. When the grating is located in a region with a monotonically varying strain, such as regions (I) or (II) in Fig. 2 (b), the Bragg resonance wavelength can be described as:

$$\lambda_B(s) = 2 \bullet n_{eff} \bullet \Lambda_0(1 + \varepsilon_i(s))$$
 (2)

where Λ_0 is the period of the uniform grating, n_{eff} is the effective reflective index of the fundamental mode in the grating region, and $\varepsilon_i(z)$ is the strain at position s along the grating.

Using coupled-mode theory and the transfer matrix method, the reflection characteristics of the uniform grating under strain gradient (I) were simulated. The parameters for this simulation included a grating pitch of 2.067 μm , a grating length of 7.5 mm, a bending orientation of 0°, a curvature radius of 2 cm, a refractive index of 1.502, and a refractive index modulation of 2.5×10^{-4} . Under strain gradient (I), the grating period monotonically decreased from 2.072 μm to 2.065 μm . The calculated reflection spectrum and group delay, shown in Fig. 2(d), confirmed the presence of a chirped fiber Bragg grating. It is important to note that both the bending orientation and curvature are constant

along the fiber, resulting in a two-dimensional shape. Furthermore, the continuous variation in the bending orientation and curvature can provide a 3D shape. This allows for diverse strain distribution and chirped characteristics to be achieved by designing the 3D shape of the fiber

3. Results and discussion

3.1. Experimental and measurement setup

The experimental setup for chromatic dispersion control and the simplified OFDR-based demodulation system are shown in Fig. 3. In the experiment, seven uniform gratings were inscribed at the same position within the HMCF. Each grating had a period of 2.067 μm and a length of 7.5 mm. The tunable chirped characteristics of the FBGs were adjusted using the setup shown in Fig. 3(b). The HMCF was fixed with a pair of fiber rotators with a scale interval of 2° , and the gratings were embedded into a semicircular groove. To adjust the bending orientation, both holders were rotated simultaneously but in opposite directions. When the upper rotator was turned clockwise, it followed the spiral direction of the HMCF. The gratings were placed into grooves of varying radii to change the curvature.

The reflected spectrum and GD of an FBG were measured using the OFDR system. The principle of OFDR-based demodulation system is illustrated in Fig. 3(a). A tunable laser source was employed, sweeping from 1525.0 nm to 1610.2 nm at a rate of 25 nm/s. Both P-polarized and S-polarized signals reflected from the FBG were collected using a polarization diversity acquisition device. The parameters of the FBG were extracted as follows: Firstly, the distribution of the FBG in distance domain was obtained by applying a fast Fourier transform (FFT) to the collected time-domain data. Then, the center position of the FBG was located based on the high reflection intensity in the distance domain. With the center position identified, and using a window length equal to the grating length, the reflection intensity of the grating was multiplied by a Hamming window. Applying an inverse fast Fourier transform (IFFT) to this data provided the reflected spectrum of the FBG.

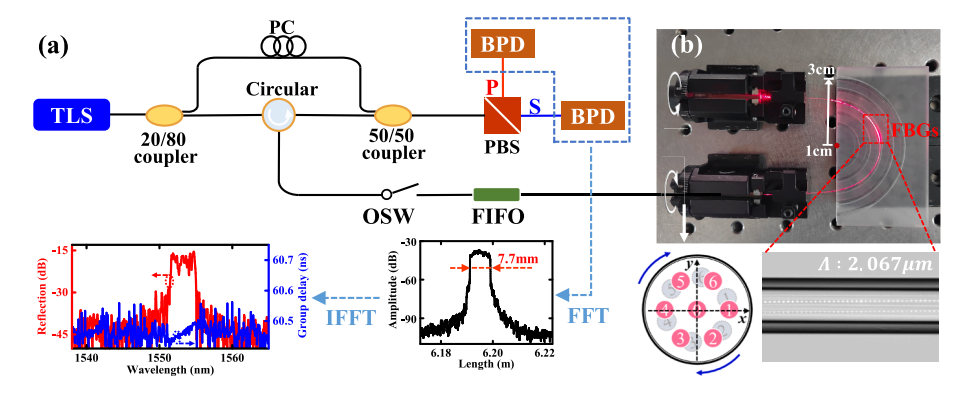


Fig. 3. (a) Schematic of simplified OFDR-based demodulation system. TLS: tunable laser source; PC: polarization controller; BPD: balanced photo-detector; PBS: polarization beam splitter; OSW: optical switch. (b) Experimental setup for chromatic dispersion control.

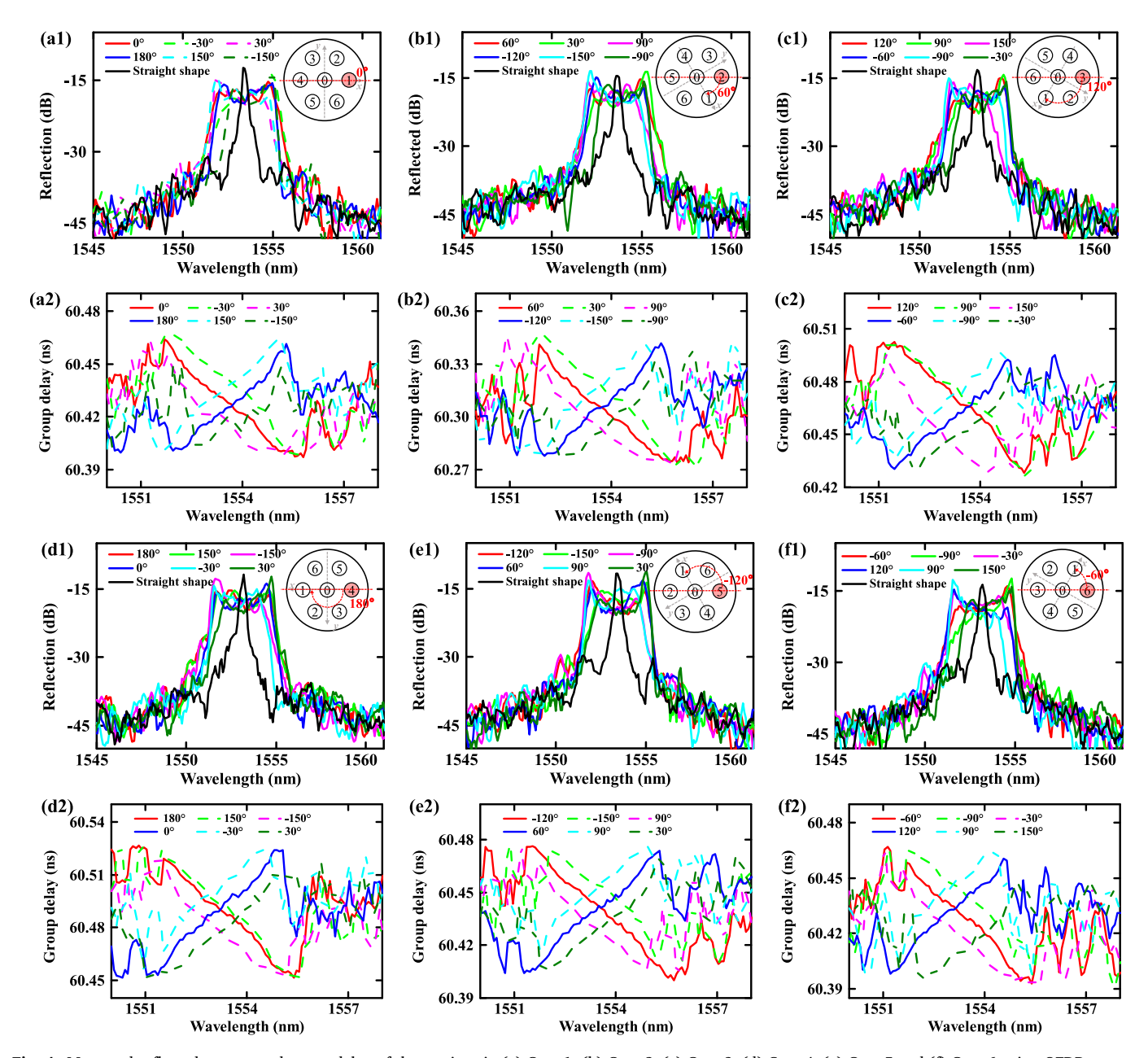


Fig. 4. Measured reflected spectra and group delay of the gratings in (a) Core-1, (b) Core-2, (c) Core-3, (d) Core-4, (e) Core-5 and (f) Core-6 using OFDR system, when the bending orientation was changed from -180° to 180° .

Meanwhile, the GD was calculated in spectral domain using the following formula:

$$\tau = \frac{\angle \left\{ i_s(v) \bullet i_s^*(\nu + \Delta \nu) + i_p(v) \bullet i_p^*(\nu + \Delta \nu) \right\}}{\Delta \nu}$$
(3)

where $i_s(v)$ and $i_p(v)$ represent the complex reflectivity at the instantaneous frequency v for P-polarized and S-polarized signals, respectively. Δv is the frequency resolution and the symbol $\angle\{\blacksquare\}$ represents an operation that calculates the phase of the complex data.

3.2. Experimental results and discussion

The influence of the bending orientation on the reflected spectrum and GD was investigated, and the results are shown in the Fig. 4. The HMCF was embedded into a concave groove with a 2.5 cm radius, and two rotators were used to change the bending orientation. Two rotators were turned clockwise and counterclockwise, respectively, to vary the bending orientation from -180° to 180° . Gratings in the seven cores were measured every 30° using the OFDR system. It is important to note that the bending orientation where the grating in Core-1 exhibited the widest spectrum was defined as 0° , corresponding to a monotonically increasing strain gradient.

As shown in Fig. 4, when the fiber was straight, the periods of all seven gratings remained constant, and they behaved as typical Bragg gratings with a linewidth of approximately 0.28 nm. However, when the fiber was bent into arcs with different curvatures, the spectra of the gratings broadened, displaying characteristics of CFBG. Specifically, at a bending orientation of 0°, the FBG in Core-1 had a bandwidth of 2.70 nm and a negative dispersion of -16.8 ps/nm. Conversely, at a 180° bending orientation, this FBG exhibited a positive dispersion of 16.2 ps/ nm, with the same bandwidth. For other bending orientations, the flat spectrum transitions to a sloping profile, resulting in an asymmetrical shape where one side rises while the other side decreases. This observation also suggests that, to ensure the grating remains within the monotonic strain region and exhibits chirped characteristics, we can shorten the grating length to mitigate the impact of the precision of the rotator. Because the included angle of two adjacent cores is 60°, the FBG in different cores did not exhibit identical characteristics. This angular offset resulted in a non-monotonic strain gradient. For instance, as shown in Fig. 4(b), at a bending orientation of 60°, matching the included angle of Core-1 and Core-2, the dispersion characteristics of the FBG in Core-2 aligned with those of Core-1. Similarly, when the bending orientation equaled the included angle of other cores and Core-1, their dispersion characteristics also matched those of Core-1, as shown in Fig. 4(c-f). This indicates that uniform gratings inscribed at the same position in the fiber do not share identical tunable dispersion characteristics.

It is worth noting that the group delay curves at bending orientations of 0° and 180° were not perfectly aligned within the same bandwidth. This is due to temperature fluctuations during the measurement period, which cause a shift in the tuning range. The shape of the fiber did not affect the resonance wavelength of the FBG in the central core (Core-7); only temperature changes caused the wavelength shift. The spectrum of the FBG in the central core was monitored throughout the experiment. As shown in Fig. 5(a), the wavelength shift spanned a range of approximately 0.4 nm, which corresponds closely to the shift in the tuning range.

The influence of curvature on the reflected spectrum and GD was also studied, and the results are shown in Fig. 6. The HMCF was embedded in concave grooves with radii of 1.0 cm, 1.5 cm, 2.0 cm, 2.5 cm, and 3.0 cm, respectively. Since the characteristics of FBG depend on both the angular offset of the cores and the bending orientation, we focused solely on the effect of curvature in this experiment. The fiber was rotated such that the grating in Core-6 experienced a monotonically decreasing strain gradient.

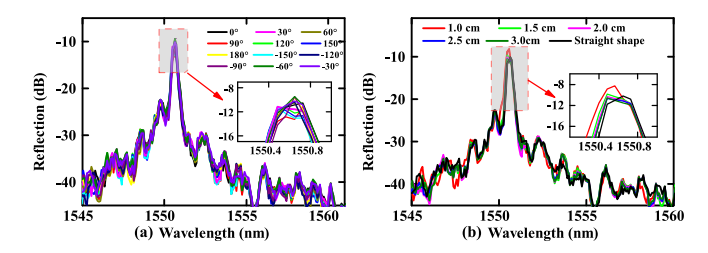


Fig. 5. Measured reflected spectra of the gratings in central Core-7 (a) throughout the bending orientation changing process and (b) curvature changing process.

As the curvature radius decreased, the reflected spectra of the gratings broadened, and the slope of the group delay curve flattened. Fig. 6 (a) shows the experimental results of the reflected spectra for the FBG with varying curvature radii. With a curvature radius of 1.0 cm, the bandwidth of the grating increased by 8.3 nm, and its reflection decreased by \sim 7.9 dB at the central wavelength of 1553.257 nm. Fig. 6 (b) shows the measured GD of the FBG for different curvature radii. Linear fitting was applied to the measured GD, and the R2 values exceeded 0.98. The slope of the fitted curves, representing the dispersion, is shown in Fig. 6(c). As the radius increased, the grating's dispersion rose from 5.7 ps/nm at 1 cm to 19.5 ps/nm at 6 cm.

Furthermore, a misalignment fabrication method was proposed to ensure that gratings in different cores exhibit identical tunable dispersion characteristics, regardless of the bending orientation, but only related to the curvature. According to the geometric characteristics of the HMCF, gratings in different cores were offset by a length ΔL ensuing consistent angular offset at the local coordinate:

$$\Delta L = \frac{\Delta \theta}{2\pi} h \tag{4}$$

where $\Delta\theta$ is the included angle of two cores. As shown in Fig. 7(a), two uniform gratings were inscribed in Core-2 and 5, respectively, with an offset of h/2. The grating length was 4.4 mm and the offset was 7.7 mm. A section of the fiber was then wound into a ring, and the bending orientation was adjusted by repositioning the gratings on the ring, as shown in Fig. 7(b). The results, shown in Fig. 7(c-d), demonstrated that these two tunable FBG had nearly identical tuning ranges and dispersion. Linear fitting of the data revealed that the dispersion for the two gratings was -6.1 ps/nm and -7.2 ps/nm, respectively.

Table 1 lists the performance of the proposed CFBG and some CFBG reported in the literature. While the fabrication of tunable and nontunable chirped gratings in SMF was well-established, the realization of CFBG in multicore fibers is still in the early stages of research. The proposed tunable CFBG, fabricated using femtosecond laser technology, was the first of its kind. Compared to the UV laser-based approach, the method proposed in this paper is more flexible, as it does not require custom phase masks. In comparison with parameters reported in the literature, the chirped grating in this work demonstrates comparable performance, with the added benefit of tunability.

4. Conclusion

In summary, we proposed and experimentally demonstrated a simple method for controlling chromatic dispersion using uniform FBGs in HMCF. By precisely adjusting the 3D shape of the grating, i.e., the local curvature and bending orientation along the fiber, we achieved effective control over key properties of the uniform FBGs, such as bandwidth and group delay. Additionally, we introduced a misalignment fabrication method to ensure that gratings in different cores exhibit consistent tunable dispersion characteristics when the fiber is bent into the same shape. In this paper, we focused solely on the tunability of the chirped characteristics of the uniform grating in HMCF induced by its 3D shape. In future work, twisting will also be investigated as a potential tuning

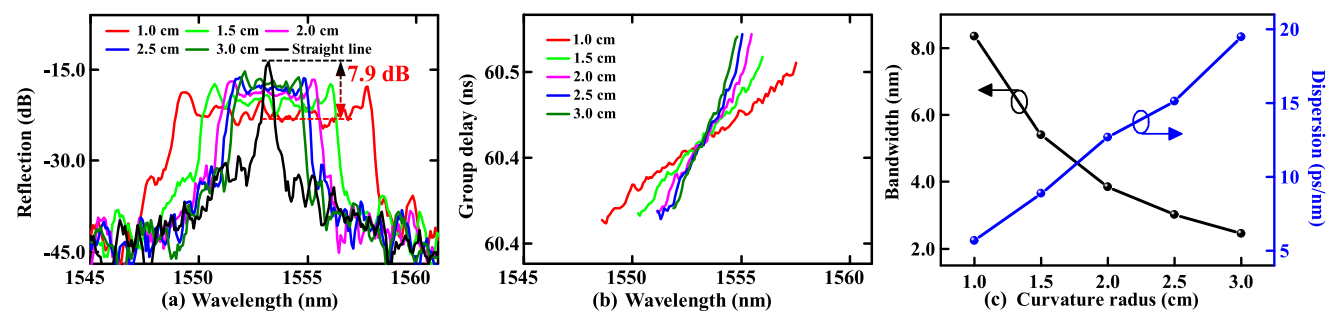


Fig. 6. Measured (a) reflected spectra and (b) group delay of the gratings in Core-6. (c) Statistics of bandwidth and dispersion with the curvature radius changed from 1 cm to 3 cm.

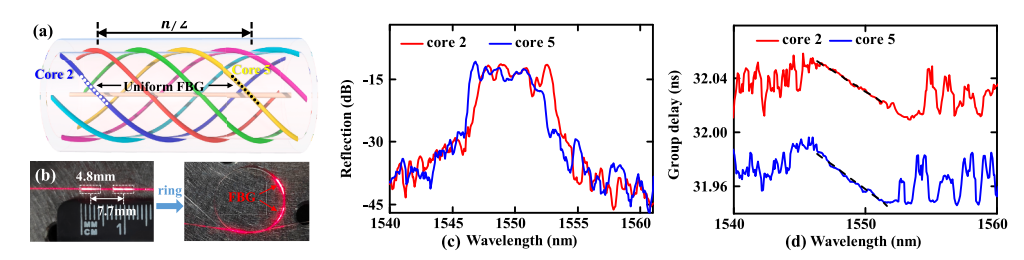


Fig. 7. (a) Schematic diagram of the gratings inscribed by misalignment method. (b) The photograph of two gratings and they were winded into a ring to be endowed chromatic dispersion-tuning property. Measured (c) reflected spectra and (d) group delay of the gratings in Core-2 and 5.

 Table 1

 Performance comparison with CFBG reported in the literature.

Fiber type	Manufacturing method	Tunability	Grating length	Bandwidth (nm)	Dispersion (ps/nm)	Refs.
SMF	UV-laser/ uniform PM	Tunable	11 cm	0.5–7.5	_	[17]
SMF	Fs-laser/ chirped PM	Non-Tunable	45 mm	4.7	_	[32]
SMF	Fs-laser/LbL	Non-Tunable	10 mm	1.5-7.7	_	[33]
MCF	UV-laser/ chirped PM	_	7 mm	1.75	_	[21]
HMCF	Fs-laser/PbP	Tunable	7.5 mm	0.28-8.3	5.7–19.5	This work

method. This proposed dispersion tuning method holds potential for applications in optical transmission systems utilizing multicore fiber.

CRediT authorship contribution statement

Yanjie Meng: Writing – review & editing, Writing – original draft, Methodology, Investigation, Funding acquisition, Data curation. Wenfa Liang: Software, Formal analysis. Zhenwei Peng: Formal analysis. Shuai Xiao: Formal analysis. Rongyi Shan: Software, Methodology. Huajian Zhong: Formal analysis. Yuhao Kong: Software. Cailing Fu: Writing – review & editing, Supervision, Conceptualization. Changrui Liao: Supervision. Zhicai Zhang: Supervision. Yiping Wang: Supervision, Funding acquisition.

Declaration of competing interest

The authors declare that they have no known competing financial interests or personal relationships that could have appeared to influence the work reported in this paper.

Acknowledgments

This work was supported by National Key Research and Development Program of China (2022YFE0111400), National Natural Science Foundation of China (grant nos. U22A2088, 62375178, 62122057), Postdoctoral Fellowship Program of CPSF (grant nos. GZC20231715,

2024 M752106), Shenzhen Key Laboratory of Ultrafast Laser Micro/Nano Manufacturing ZDSYS(20220606100405013), Shenzhen Science and Technology Program (JCYJ20220818095800001), LingChuang Research Project of China National Nuclear Corporation (No. CNNC-LCKY-202265).

Data availability

Data will be made available on request.

References

- D.J. Richardson, J.M. Fini, L.E. Nelson, Space-division multiplexing in optical fibres, Nat. Photonics 7 (5) (2013) 354–362.
- [2] R.G.H. van Uden, R.A. Correa, E.A. Lopez, F.M. Huijskens, C. Xia, G. Li, A. Schülzgen, H. de Waardt, A.M.J. Koonen, C.M. Okonkwo, Ultra-high-density spatial division multiplexing with a few-mode multicore fibre, Nat. Photonics 8 (11) (2014) 865–870.
- [3] R. Ryf, S. Randel, A.H. Gnauck, C. Bolle, A. Sierra, S. Mumtaz, M. Esmaeelpour, E. C. Burrows, R.J. Essiambre, P.J. Winzer, D.W. Peckham, A.H. McCurdy, R. Lingle, Mode-division multiplexing over 96 km of few-mode fiber using coherent 6 x 6 MIMO processing, J. Lightwave Technol. 30 (4) (2012) 521–531.
- [4] R.W. Tkach, Scaling optical communications for the next decade and beyond, Bell Labs Tech. J. 14 (4) (2010) 3–9.
- [5] B.J. Puttnam, R.S. Luis, I. Phillips, M. Tan, A. Donodin, D. Pratiwi, L. Dallachiesa, Y. Huang, M. Mazur, N.K. Fontaine, H. Chen, D. Chung, V. Ho, D. Orsuti, B. Boriboon, G. Rademacher, L. Palmieri, R. Man, R. Ryf, D.T. Neilson, W. Forysiak, H. Furukawa, 402 Tb/s GMI data-rate OESCLU-band transmission, Opt.Fiber Commun. Conf. Exhibition (OFC) 2024 (2024) 1–3.

- [6] B. Zhu, T.F. Taunay, M. Fishteyn, X. Liu, S. Chandrasekhar, M.F. Yan, J.M. Fini, E. M. Monberg, F.V. Dimarcello, K. Abedin, P.W. Wisk, D.W. Peckham, P. Dziedzic, Space-, wavelength-, polarization-division multiplexed transmission of 56-TB/s over a 76.8-km seven-core fiber. 2011 Optical Fiber Communication Conference and Exposition (ofc/nfoec) and the National Fiber Optic Engineers Conference, 2011.
- [7] R. Ryf, R.J. Essiambre, A.H. Gnauck, S. Randel, M.A. Mestre, C. Schmidt, P. J. Winzer, R. Delbue, P. Pupalaikis, A. Sureka, T. Hayashi, T. Taru, T. Sasaki, Space-division multiplexed transmission over 4200-km 3-core microstructured fiber, OFC/NFOEC (2012) 1–3.
- [8] T.F. Hussein, M.R.M. Rizk, M.H. Aly, A hybrid DCF/FBG scheme for dispersion compensation over a 300km SMF, Opt. Quant. Electron. 51 (4) (2019).
- [9] Z.W. Tan, Y.H. Wang, W.H. Ren, Y. Liu, B. Li, T.G. Ning, S.S. Han, Transmission system over 3000 km with dispersion compensated by chirped fiber Bragg gratings, Optik 120 (1) (2009) 9–13.
- [10] B.J. Eggleton, J.A. Rogers, P.S. Westbrook, T.A. Stresser, Electrically tunable power efficient dispersion compensating fiber Bragg grating, IEEE Photonic. Tech. L. 11 (7) (1999) 854–856.
- [11] N.Q. Ngo, S.Y. Li, R.T. Zheng, S.C. Tjin, P. Shum, Electrically tunable dispersion compensator with fixed center wavelength using fiber Bragg grating, J. Lightwave Technol. 21 (6) (2003) 1568–1575.
- [12] L. Dong, J.L. Cruz, L. Reekie, J.A. Tucknott, Fabrication of chirped fiber gratings using etched tapers, Electron Lett. 31 (11) (1995) 908–909.
- [13] J. Mora, A. Díez, M.V. Andrés, P.Y. Fonjallaz, M. Popov, Tunable dispersion compensator based on a fiber Bragg grating written in a tapered fiber, IEEE Photon. Tech. L. 16 (12) (2004) 2631–2633.
- [14] H. Liu, S.C. Tjin, N.Q. Ngo, K.B. Tan, K.M. Chan, J.H. Ng, C. Lu, A novel method for creating linearly and nonlinearly chirped fiber Bragg gratings, Opt. Commun. 217 (1–6) (2003) 179–183.
- [15] C.S. Goh, S.Y. Set, K. Kikuchi, Design and fabrication of a tunable dispersion-slope compensating module based on strain-chirped fiber Bragg gratings, IEEE Photon. Tech. L. 16 (2) (2004) 524–526.
- [16] Y.G. Han, S.B. Lee, Tunable dispersion compensator based on uniform fiber Bragg grating and its application to tunable pulse repetition-rate multiplication, Opt. Express 13 (23) (2005) 9224–9229.
- [17] Y.J. Lee, J. Bae, K. Lee, J.M. Jeong, S.B. Lee, Tunable dispersion and dispersion slope compensator using strain-chirped fiber Bragg grating, IEEE Photon. Tech. L. 19 (9–12) (2007) 762–764.
- [18] E. Lindley, S.S. Min, S. Leon-Saval, N. Cvetojevic, J. Lawrence, S. Ellis, J. Bland-Hawthorn, Demonstration of uniform multicore fiber Bragg gratings, Opt. Express 22 (25) (2014) 31575–31581.
- [19] M. Becker, A. Lorenz, T. Elsmann, I. Latka, A. Schwuchow, S. Dochow, R. Spittel, J. Kobelke, J. Bierlich, K. Schuster, M. Rothhardt, H. Bartelt, Single-mode

- multicore fibers with integrated Bragg filters, J. Lightwave Technol. 34 (19) (2016) 4572–4578
- [20] M.X. Hou, K.M. Yang, J. He, X.Z. Xu, S. Ju, K.K. Guo, Y.P. Wang, Two-dimensional vector bending sensor based on seven-core fiber Bragg gratings, Opt. Express 26 (18) (2018) 23770–23781.
- [21] S.G. Kilic, Y.P. Zhu, Q.W. Sheng, M.N. Inci, M. Han, Refractometer with etched chirped fiber Bragg grating fabry-perot interferometer in multicore fiber, IEEE Photon. Tech. L. 31 (8) (2019) 575–578.
- [22] X.F. Zhao, X. Tian, M. Wang, H.Y. Li, B.Y. Rao, Z.F. Wang, Design and fabrication of wideband chirped tilted fiber Bragg gratings, Opt. Laser Technol. 148 (2022).
- [23] A. Martinez, M. Dubov, I. Khrushchev, I. Bennion, Direct writing of fibre Bragg gratings by femtosecond laser, Electron Lett. 40 (19) (2004) 1170–1172.
- [24] K.M. Zhou, M. Dubov, C.B. Mou, L. Zhang, V.K. Mezentsev, I. Bennion, Line-by-line fiber Bragg grating made by femtosecond laser, IEEE Photon. Tech. L. 22 (16) (2010) 1190–1192.
- [25] A. Theodosiou, A. Lacraz, M. Polis, K. Kalli, M. Tsangari, A. Stassis, M. Komodromos, Modified fs-laser inscribed FBG array for rapid mode shape capture of free-free vibrating beams, IEEE Photon. Tech. L. 28 (14) (2016) 1502-1512
- [26] J. He, B.J. Xu, X.Z. Xu, C.R. Liao, Y.P. Wang, Review of femtosecond-laser-inscribed fiber bragg gratings: fabrication technologies and sensing applications, Photon. Sens. 11 (2) (2021) 203–226.
- [27] A. Donko, M. Beresna, Y. Jung, J. Hayes, D.J. Richardson, G. Brambilla, Point-by-point femtosecond laser micro-processing of independent core-specific fiber Bragg gratings in a multi-core fiber, Opt. Express 26 (2) (2018) 2039–2044.
- [28] A. Wolf, A. Dostovalov, K. Bronnikov, S. Babin, Arrays of fiber Bragg gratings selectively inscribed in different cores of 7-core spun optical fiber by IR femtosecond laser pulses, Opt. Express 27 (10) (2019) 13978–13990.
- [29] Y.J. Meng, S. Xiao, R.Y. Shan, W.F. Liang, H.J. Zhong, Y.H. Kong, Z.W. Peng, C. L. Fu, C.R. Liao, Z.C. Zhang, Y.P. Wang, Length-extended 3D shape sensor using wavelength/space-division multiplexing grating arrays in a multicore fiber, Opt. Lett. 49 (15) (2024) 4146–4149.
- [30] B.J. Soller, D.K. Gifford, M.S. Wolfe, M.E. Froggatt, High resolution optical frequency domain reflectometry for characterization of components and assemblies, Opt. Express 13 (2) (2005) 666–674.
- [31] J.P. Moore, M.D. Rogge, Shape sensing using multi-core fiber optic cable and parametric curve solutions, Opt. Express 20 (3) (2012) 2967–2973.
- [32] A. Halstuch, A.A. Ishaaya, Femtosecond inscription of chirped fiber Bragg gratings and fiber Bragg grating arrays using a single uniform phase-mask, Opt. Laser Eng. 160 (2023) 107286.
- [33] T. Duan, X. Li, R. Wang, F. Chen, X. Qiao, Femtosecond laser plane-by-plane inscription of chirped and tilted fiber Bragg gratings, J. Lightwave Technol. 42 (17) (2024) 6083–6089.